Broken inversion symmetry in the charge density wave phase in $EuAl_4$

Surya Rohith Kotla,[1] Leila Noohinejad,[2] Preeti Pokhriyal,[2] Martin Tolkiehn,[2] Harshit Agarwal,[1,3] Sitaram Ramakrishnan,[4] and Sander van Smaalen[1,*]

[1]*Laboratory of Crystallography, Bayerisches Geoinstitut, University of Bayreuth, 95440 Bayreuth, Germany*
[2]*Deutsches Elektronen-Synchrotron DESY, Notkestrasse 85, 22607 Hamburg, Germany*
[3]*Institut für Physik, Johannes-Gutenberg-Universität Mainz, 55128 Mainz, Germany*
[4]*Institut Néel CNRS/UGA UPR2940, 25 Rue des Martyrs, 38042 Grenoble, France*

(Received 4 June 2025; revised 24 July 2025; accepted 15 August 2025; published 28 August 2025)

$EuAl_4$ exhibits a complex phase diagram, including the development of a charge density wave (CDW) below $T_{CDW} = 145$ K. Below $T_N = 15.4$ K, a series of antiferromagnetically (AFM) ordered phases appear, while nontrivial topological phases, like skyrmion lattices, are stabilized under an applied magnetic field. The symmetries of the variously ordered phases are a major issue concerning the understanding of the stabilization of the ordered phases as well as concerning the interplay between the various types of order. $EuAl_4$ at room temperature has tetragonal symmetry with space group $I4/mmm$. The CDW phase has an incommensurately modulated crystal structure described by the modulation wave vector $\mathbf{q} \approx 0.17\,\mathbf{c}^*$. On the basis of various experiments, including elastic and inelastic x-ray scattering, and second-harmonic generation, it has been proposed that the symmetry of the CDW phase of $EuAl_4$ could be centrosymmetric orthorhombic, noncentrosymmetric orthorhombic or noncentrosymmetric tetragonal. Here, we report temperature-dependent, single-crystal x-ray diffraction experiments that show that the CDW is a transverse CDW with phason disorder, and with noncentrosymmetric symmetry according to the orthorhombic superspace group $F222(0\,0\,\sigma)00s$. Essential for this finding is the availability of a sufficient number of second-order ($2\mathbf{q}$) satellite reflections in the x-ray diffraction data set. The broken inversion symmetry implies that skyrmions might form due to Dzyaloshinskii-Moriya (DM) interactions, instead of a more exotic mechanism as it is required for centrosymmetric structures.

DOI: 10.1103/kl2z-brms

I. INTRODUCTION

The charge density wave (CDW) was originally proposed as an instability of quasi-one-dimensional (1D) metals that is stabilized by Fermi-surface nesting (FSN) [1,2]. Since then, materials have been discovered that possess a CDW at low temperatures, but that have a three-dimensional (3D) electronic band structure. Stabilization of these CDWs is by alternate mechanisms, for example by momentum-dependent electron-phonon coupling (EPC) instead of FSN [3]. A CDW leads to a modified band structure as well as displacements of the atoms out of their lattice-periodic positions. Both the electron density and the atomic displacements are modulated in a wavelike manner. These waves are characterized by a common modulation wave vector $\mathbf{q}$, that is in general incommensurate with the underlying lattice. These features imply an interaction or competition between CDWs and other electronic properties [4]. For example, superconductivity (SC) is enhanced upon suppression of the CDW by application of pressure or chemical doping, as it has been found for $Lu_5Ir_4Si_{10}$ [5,6], and the kagome lattice compound CsV_3Sb_5 [7,8]. Several compounds $RNiC_2$ (R = rare earth) possess a CDW, while at lower temperatures magnetic order develops. The CDW coexists with antiferromagnetic (AFM) order [9,10], while the CDW disappears on entering the ferromagnetic (FM) state [11,12]. On the other hand, magnetic order is suppressed by the presence of a CDW in $Er_2Ir_3Si_5$ [13,14].

The topological magnets $EuAl_4$ and $EuAl_2Ga_2$ [15,16] have attracted attention due to the presence of CDWs and magnetic order at low temperatures [17–19]. The complex phase diagrams include four differently ordered magnetic phases below $T_N = 15.4$ K in $EuAl_4$ as well as several metamagnetic phases, including two types of skyrmion lattices under applied magnetic field [17,18]. Magnetic order develops out of the CDW phase. The symmetry of the CDW thus is of high importance for understanding the microscopic mechanism of magnetic order.

At room temperature, $EuAl_4$ has the $BaAl_4$ structure type with tetragonal symmetry $I4/mmm$ (Fig. 1). Originally, it was proposed that the symmetry of $EuAl_4$ would remain tetragonal in its CDW phase, because no lattice distortions could be observed [20]. While this observation has been confirmed in several studies by x-ray diffraction, including the present study, lower symmetries were proposed for the CDW phase, including the orthorhombic superspace groups $Fmmm(0\,0\,\sigma)s00$ and $Immm(0\,0\,\sigma)s00$ [21–24]. The

*Contact author: smash@uni-bayreuth.de

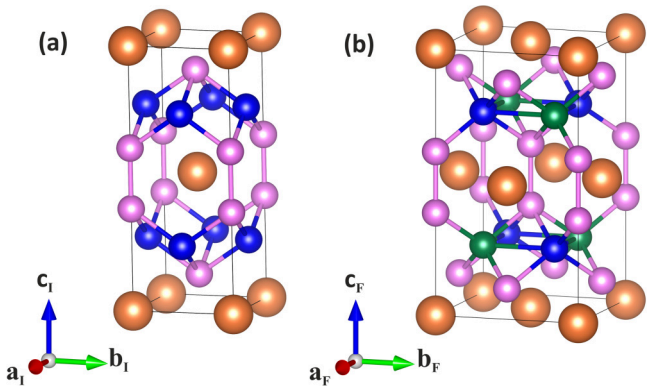

FIG. 1. (a) Crystal structure of $EuAl_4$ with space group $I4/mmm$ in the periodic phase at 160 K. Depicted is an I-centered unit cell with basis vectors $\mathbf{a}_I$, $\mathbf{b}_I$, and $\mathbf{c}_I$. (b) Basic structure of $EuAl_4$ in the CDW phase at 30 K, showing an F centered unit cell with basis vectors $\mathbf{a}_F$, $\mathbf{b}_F$, and $\mathbf{c}_F$ and space group $F222$. The relation between the I-centered and F-centered unit cells is $\mathbf{a}_F = (\mathbf{a}_I + \mathbf{b}_I)$, $\mathbf{b}_F = (-\mathbf{a}_I + \mathbf{b}_I)$, and $\mathbf{c}_F = \mathbf{c}_I$. Orange spheres correspond to the Eu atoms; blue spheres represent Al1/Al1a atoms; green spheres represent Al1b atoms; and pink spheres stand for Al2 atoms.

tetragonal point groups 4 and $4/m$ were suggested on the basis of second-harmonic-generation (SHG) measurements [25].

Here, we report the incommensurately modulated crystal structure of the CDW state of $EuAl_4$ with the noncentrosymmetric orthorhombic symmetry $F222(0\,0\,\sigma)00s$, as obtained from temperature-dependent single-crystal x-ray diffraction (SXRD). The noncentrosymmetric symmetry can only be distinguished from the previously suggested centrosymmetric superspace groups through the inclusion of second-order ($m = 2$) satellite reflections in the structural analysis. Second-order satellites were not available in previous studies [21,22]. Furthermore, the structural analysis indicates phason disorder in the CDW [26].

The present result corroborates the analysis from cryogenic four-dimensional scanning transmission electron microscopy (4D-STEM), on the basis of which a structural modulation was proposed without assigning a symmetry to it [27]. It also mirrors the symmetry obtained for the isostructural, nonmagnetic CDW compound $SrAl_4$, for which the SXRD data include second-order satellites [28].

The proposed symmetry is important for the description of the magnetically ordered phases. The noncentrosymmetric superspace group allows for a stabilization of skyrmions by Dzyaloshinskii-Moriya (DM) interactions, the latter which are usually the source of skyrmions [29–31]. A more exotic mechanism, like those involving itinerant-electron-mediated interactions, is not required [17,18,27]. Second, Vibakhar *et al.* [32] have found that the magnetic symmetry becomes polar monoclinic at the onset of the third AFM phase, while the symmetry of the CDW would lower to point group 222 or 2. The present result of the noncentrosymmetric superspace symmetry $F222(0\,0\,\sigma)00s$ for the CDW phase demonstrate that point group 222 has already been reached, before any magnetic order develops.

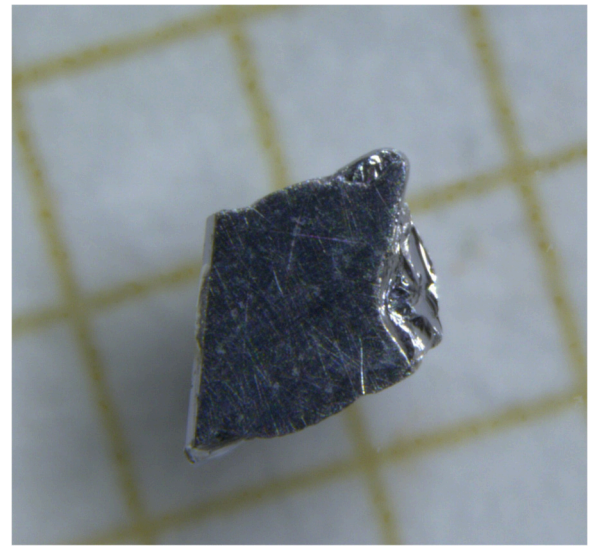

FIG. 2. Single crystal of $EuAl_4$ as separated from the Al flux. Yellow lines form a mesh of 1×1 mm^2.

II. EXPERIMENT

A. Crystal growth

High-quality single crystals of $EuAl_4$ were grown by the self-flux method according to the procedure described by Nakamura *et al.* [33], using growth parameters different from our previous work [21]. Europium (Smart-elements, 99.99% purity) and aluminum (Alfa-Aesar, 99.9995%) were mixed into an alumina crucible in the elemental ratio 1:9, and then sealed under vacuum in a quartz-glass tube. The quartz-glass tube was heated to 1173 K and maintained at this temperature for two days. It was then slowly cooled down to 673 K over 110 hours. The oven was tilted by 9°, with the materials at the lower side, thus keeping all materials together during the reaction. After cooling to room temperature, a single crystal was obtained of about 1 mm in size (Fig. 2).

We believe that the present single crystal was of better quality (fewer lattice defects) than the crystal used in our earlier study [21]. Most likely, this is due to an effective annealing of the present material, as it has resulted from the slow cooling down to 673 K, as opposed to quenching from 923 K to room temperature in [21].

B. X-ray diffraction

The as-grown single crystal was crushed, and a small part of dimensions $0.063 \times 0.041 \times 0.005$ mm^3 was selected for single-crystal x-ray diffraction (SXRD). Diffraction experiments were performed with synchrotron radiation at Beamline P24 of PETRA III at DESY in Hamburg, Germany, employing radiation of a wavelength of 0.5000 Å. A CRYOCOOL G2B-LT open-flow helium gas cryostat was used for controlling the temperature of the sample.

The SXRD data were measured by the rotation method, employing a LAMBDA 7.5 M area detector by X-Spectrum [34]. Frames of width of 0.1° and exposure time 0.1 s were collected during continuous rotation over 364°. At each temperature, the raw data were binned toward a single run of 363

frames of 1° wide. The software CrysAlisPro [35] was used for the computation of undistorted views of reciprocal space. Two complete data sets of SXRD data were obtained in this way: The SXRD-160 data for a sample temperature of 160 K, and the SXRD-30 data for a sample temperature of 30 K. In a similar way, the data from Ref. [21] are designated SXRD-250 and SXRD-70 data.

Data processing of the binned runs was performed with the EVAL15 software suite [36]. Indexing and integration resulted in values for the lattice parameters and modulation wave vector, as well as a list of Bragg reflections with their integrated intensities. Absorption correction and scaling were computed for each data set by the software SADABS [37]. These corrections are obtained through the comparison of intensities of equivalent reflections. The correction thus depends on the point symmetry that is assumed to be valid for the SXRD data. Here, the problem arises that different symmetries lead to comparable agreements between equivalent reflections, with $R_{\rm int} \approx 3\%$ for main reflections, and even slightly higher for the tetragonal phase at 160 K (see Table S1 in the Supplemental Material [38]). This can be explained by twinning of the crystal in the CDW phase, as it is likely to occur at the CDW phase transition, if this transition leads to a lowering of the point group. For equal volumes of twin domains, the diffraction data of $EuAl_4$ would have $4/mmm$ point symmetry, irrespective of the symmetry of the crystal structure in the CDW state.

Refinements of the crystal structures was done using the software package JANA2020 [39]. Details of the experiment, data processing, and crystallographic information are provided in Table I and in the Supplemental Material [38].

TABLE I. Crystallographic data of $EuAl_4$ at 160 K (periodic phase) and 30 K (CDW phase).

Temperature (K)	160	30
Crystal system	Tetragonal	Orthorhombic
(Super-)space group	$I4/mmm$	$F222(0\,0\,\sigma)00s$
No. [40]	139	22.1.17.2
a (Å)	4.3922(1)	6.2056(1)
b (Å)	4.3922	6.2055(1)
c (Å)	11.1707(3)	11.1630(2)
Volume (Å^3)	215.50(1)	429.88(2)
Wave vector **q**		$0.1743(1)\,\mathbf{c}^*$
Z	2	4
Wavelength (Å)	0.50000	0.50000
Detector distance (mm)	95	95
χ-offset (deg)	−60	−60
Rotation per frame (deg)	1	1
$(\sin(\theta)/\lambda)_{\rm max}$ (Å^{-1})	0.719972	0.720842
Absorption coefficient, μ (mm^{-1})	5.875	5.890
$T_{\rm min}$, $T_{\rm max}$	0.7057, 0.8618	0.6794, 0.8618
Criterion of observability	$I > 3\sigma(I)$	$I > 3\sigma(I)$
No. of reflections measured,		
$(m = 0)$	1796	1144
$(m = 1)$		2316
$(m = 2)$		2322
Point group for averaging	$4/mmm$	mmm
No. of unique reflections,		
$(m = 0)$ (obs/all)	127/127	207/207
$(m = 1)$ (obs/all)		345/380
$(m = 2)$ (obs/all)		31/394
$R_{\rm int}$ (obs/all)	0.0386/0.0386	0.0407/0.0414
$R_{\rm int}(m = 0)$ (obs/all)	0.0386/0.0386	0.0303/0.0303
$R_{\rm int}(m = 1)$ (obs/all)		0.1056/0.1063
$R_{\rm int}(m = 2)$ (obs/all)		0.1653/0.2325
No. of parameters	9	40
$R_F(m = 0)$ (obs)	0.0193	0.0167
$R_F(m = 1)$ (obs)		0.0416
$R_F(m = 2)$ (obs)		0.0566
$wR_F(m = 0)$ (all)	0.0230	0.0204
$wR_F(m = 1)$ (all)		0.0477
$wR_F(m = 2)$ (all)		0.1921
wR_F (all) (all refl.)	0.0230	0.0317
GoF (obs/all)	1.71/1.71	1.37/1.11
$\Delta\rho_{\rm min}$, $\Delta\rho_{\rm max}$(e Å^{-3})	−1.35, 1.39	−4.6, 5.24

III. SYMMETRY AND CRYSTAL STRUCTURE

The diffraction data at 160 K (SXRD-160 data) confirm the $BaAl_4$ structure type with space group $I4/mmm$ for $EuAl_4$ [41]. Structure refinements led to an excellent fit to the SXRD-160 data with $R_F = 0.0193$ (Table I). Parameters of the three crystallographically independent atoms—Eu, Al1, and Al2—are given in Table S6 in the Supplemental Material [38].

Cooling of the crystal toward 30 K resulted in the appearance of satellite reflections in the SXRD [20]. The observation of up to third-order satellite reflections has been reported in the literature, but only first-order satellite reflections have been used for structural analysis [20–22]. Presently, the SXRD-30 data comprise both first-order and second-order satellite reflections (Fig. 3 and Table S1 in [38]).

The incommensurately modulated crystal structure of $EuAl_4$ in its CDW state is described within the superspace approach [42,43]. In principle, any superspace group is a candidate symmetry for the CDW phase, which is based on a modulation wave vector along $\mathbf{c}^*$ and a basic-structure space group that is a "translationsgleiche" subgroup of $I4/mmm$. A total of 63 superspace groups exist with these properties [28]. Previous analyses of SXRD data of up to first-order satellites have shown that six of these 63 superspace groups allow for a structure model that may describe the SXRD data well [21,22,28]. Present refinements confirm this finding for the SXRD-30 data (Tables S2 and S3 in [38]). These symmetries comprise two acentric tetragonal superspace groups, two acentric orthorhombic superspace groups, and two centrosymmetric orthorhombic superspace groups (Fig. 4 and Table II).

The goal of the present analysis is to determine the symmetry and crystal structure of the CDW phase. First, it is noticed that the lattice remains of tetragonal metric in the CDW phase. No splitting nor broadening has been observed of Bragg reflections (Fig. 3), in agreement with the literature [20–22,25]. This observation indicates that the lattice symmetry remains tetragonal within experimental error. However, as shown below, the symmetry of the crystal structure is lowered to acentric orthorhombic in the CDW phase.

The first model to be considered is the basic structure (no modulation). Except for $I4$, the basic-structure coordinates remain equal to those of $I4/mmm$, where there exists only

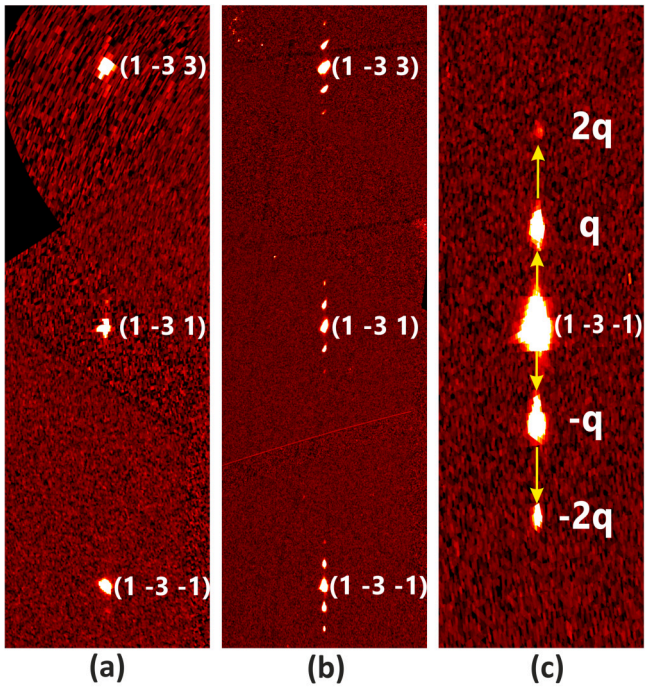

FIG. 3. Undistorted view of the $(1\,k\,l)$ reciprocal lattice plane of (a) the SXRD-160 data, and (b) the SXRD-30 data. (c) Enlarged view of panel (b) about reflection $(1\,{-}3\,{-}\,1)$, with clearly visible first-order and second-order satellite reflections. Images have been generated from the measured data by the software CrysAlisPro [35]. Dark bands are due to gaps (insensitive area) between the active modules of the Lambda 7.5M area detector.

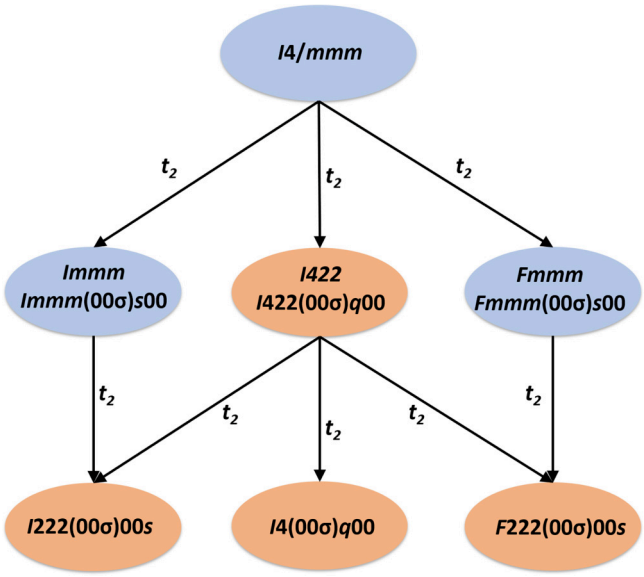

FIG. 4. Flow chart showing the relations between tetragonal and orthorhombic space groups and superspace groups, where the basic-structure space group is a subgroup of $I4/mmm$. Furthermore, the acentric orthorhombic superspace groups (bottom row) are subgroups of the superspace groups in the middle row. "t2" indicates that the point group is a subgroup of index two. Centrosymmetric superspace groups are in light blue and acentric superspace groups are in light brown color.

one refinable coordinate, z[Al2] (Table S6 in [38]). A special case is the symmetry $F222(0\,0\,\sigma)00s$, in which the Al1 site splits into two sites, denoted as Al1a and Al1b. Since Al1, Al1a, and Al1b do not incorporate refinable coordinates, the symmetry of the basic structure remains $I4/mmm$ here too. The orthorhombic symmetries do allow for more independent ADP parameters. However, lower symmetry for the ADPs is unlikely for an undistorted basic structure. Therefore, the basic-structure ADPs were restricted to follow $I4/mmm$ symmetry in all refinements. An excellent fit of the main reflections of the SXRD-30 data has been obtained (Table II). These results imply that the basic structure of the incommensurate CDW phase remains tetragonal, and that any distortions will be due to the modulation wave. The less good agreement for the I-centered orthorhombic symmetry is attributed to the less than optimal performance of the SADABS refinement for this symmetry.

The second model describes the displacive modulation by first-order harmonic parameters. Although a reasonable fit to the SXRD-30 data is obtained for all six symmetries, except for the fit to the second-order satellite reflections for models with centrosymmetric symmetries (Table II), several problems remain. First, the fit to the main reflections is less good than in the basic-structure refinement. However, this fit should improve upon the introduction of the correct model for the incommensurate modulation. Apparently, something is lacking for this model. In this respect, it is noticed that the standard procedure would be the introduction of second-order harmonic parameters for the displacement modulation, if the SXRD data contain second-order satellite reflections, as the SXRD-30 data do. However, the second problem with the simple modulated structure is that second-order satellite reflections are calculated too strong, i.e.,

$$\Delta F(h\,k\,l\,m) = (F_{\rm obs}(h\,k\,l\,m) - F_{\rm cal}(h\,k\,l\,m)) < 0 \qquad (1)$$

for most second-order satellites ($m = \pm 2$). We have called this the ΔF problem, and it is found for all symmetries (Table II). Nonzero values for the second-order harmonic parameters for the displacive modulation lead to even higher calculated structure factor amplitudes $F_{\rm cal}(h\,k\,l\,m)$ for the second-order satellites, aggravating the ΔF problem. Indeed, refinements of the displacement modulation up to second-order harmonic parameters leads to insignificant or zero values for the latter.

Instead of modifying the displacement modulation functions, modulations can be introduced for the ADPs. First-order harmonic parameters for the modulation of the ADPs did not lead to an improved fit to the SXRD-30 data, while those parameters refined to values smaller than their standard uncertainties. Therefore, we have restricted to zero the values of these parameters in the remaining analysis. The third model that we have considered is the combination of first-order harmonic parameters for displacive modulation with second-order harmonic parameters for the modulation of ADPs. A clearly improved fit to the SXRD-30 data was thus obtained for five out of six superspace symmetries (Table II), while the ΔF problem is resolved. However, we

TABLE II. Structure refinements against the SXRD-30 data of $EuAl_4$ in its incommensurate CDW phase at $T = 30$ K. Three types of structure model are considered for each of six superspace symmetries. "Basic structure" refers to a refinement of the basic structure against main reflections ($m = 0$) only; "Displacement modulation" adds to the basic structure first-order harmonic modulation parameters of displacement modulation; "Displacement + ADP modulation" adds to "displacement modulation" second-order harmonic modulation parameters for the anisotropic displacement parameters (ADPs). SXRD-30 data have been processed according to the centrosymmetric point group of the superspace group (Table S1 in [38]). Criterion of observability is $I > 3\sigma(I)$. n_{par} is the number of refined parameters. "*" indicates refinements with a ΔF problem (see text).

SSG	Averaging	n_{par}	R_F^{obs} (Overall) (%)	R_F^{obs} ($m = 0$) (%)	R_F^{obs} ($m = 1$) (%)	R_F^{obs} ($m = 2$) (%)
			Basic structure			
$I422(0\,0\,\sigma)q00$	$4/mmm$	9	1.79	1.79		
$I4(0\,0\,\sigma)q00$	$4/m$	11	1.68	1.68		
$Immm(0\,0\,\sigma)s00$	$Immm$	9	3.24	3.24		
$I222(0\,0\,\sigma)00s$	$Immm$	9	3.24	3.24		
$Fmmm(0\,0\,\sigma)s00$	$Fmmm$	9	1.81	1.81		
$F222(0\,0\,\sigma)00s$	$Fmmm$	9	1.81	1.81		
			Displacement modulation			
$I422(0\,0\,\sigma)q00$	$4/mmm$	14*	3.37	2.12	6.12	4.59
$I4(0\,0\,\sigma)q00$	$4/m$	21*	3.31	1.94	6.03	4.74
$Immm(0\,0\,\sigma)s00$	$Immm$	14*	4.81	3.36	7.37	20.31
$I222(0\,0\,\sigma)00s$	$Immm$	19*	4.28	3.31	6.39	3.85
$Fmmm(0\,0\,\sigma)s00$	$Fmmm$	15*	4.14	2.21	7.58	23.63
$F222(0\,0\,\sigma)00s$	$Fmmm$	19*	3.5	2.05	6.5	4.9
			Displacement + ADP modulation			
$I422(0\,0\,\sigma)q00$	$4/mmm$	24	3.37	2.1	6.01	7.55
$I4(0\,0\,\sigma)q00$	$4/m$	41	2.93	1.79	5.05	8.23
$Immm(0\,0\,\sigma)s00$	$Immm$	29	4	3.32	5.13	13.09
$I222(0\,0\,\sigma)00s$	$Immm$	40	3.63	3.17	4.57	5.19
$Fmmm(0\,0\,\sigma)s00$	$Fmmm$	28	2.86	1.81	4.78	12.05
$F222(0\,0\,\sigma)00s$	$Fmmm$	40	2.51	1.67	4.16	5.66

notice that the best fit with $R_F^{\mathrm{obs}}(\mathrm{overall}) = 2.51\%$ is obtained for the noncentrosymmetric orthorhombic superspace group $F222(0\,0\,\sigma)00s$. Furthermore, the two tetragonal superspace groups lead to higher values for $R_F^{\mathrm{obs}}(m = 0)$ than in the basic-structure refinement; an additional argument against these symmetries. Both centrosymmetric orthorhombic superspace groups—previously proposed on the basis of SXRD data without second-order satellites [21,22,28]—can be excluded, because of the poor fit to the second-order satellite reflections.

An alternate approach is to use the same reflection list for all refinements. This list then should be based on the common point symmetry of all six superspace groups, which is **c**-unique monoclinic symmetry. Accordingly, SXRD-30 data have been processed within $2/m$ point symmetry with, apparently, similar results as for processing within the other symmetries (Table S1 in [38]). However, refinements show a less good fit to the main reflections, indicating that the computation of the absorption correction and other scalings was less successful for $2/m$ symmetry than for the higher symmetries, probably because of the lower redundancy for $2/m$ symmetry. Nevertheless, with these data, $F222(0\,0\,\sigma)00s$ is marginally preferred over $I222(0\,0\,\sigma)00s$ (Table S4 in [38]). We attribute this very small difference to the almost perfect twinning (all domains of equal volume) of the crystal while measuring the SXRD-30 data. With inversion twins restricted to be equal, refined twin volumes are 0.253(2):0.247 for $I222(0\,0\,\sigma)00s$ and 0.257(2):0.243 for $F222(0\,0\,\sigma)00s$ symmetry. The SXRD-70 data were measured on a different crystal that appeared to be twinned with twin volumes 0.29:0.21. This deviation from perfect twinning has appeared to be sufficient for a more clear preference of $F222(0\,0\,\sigma)00s$ over $I222(0\,0\,\sigma)00s$ symmetry, despite the lack of second-order satellites (Table III and Table S5 in [38]).

IV. DISCUSSION

The symmetry of the CDW state of $EuAl_4$ has been found as noncentrosymmetric orthorhombic with superspace group $F222(0\,0\,\sigma)00s$. This superspace group is a subgroup of centrosymmetric $Fmmm(0\,0\,\sigma)s00$, which was previously proposed as symmetry [21]. Alternatively, the other centrosymmetric orthorhombic superspace group, $Immm(0\,0\,\sigma)s00$, was proposed as symmetry [22] (Fig. 1). Here, the I-centered orthorhombic groups preserve the twofold axes along the

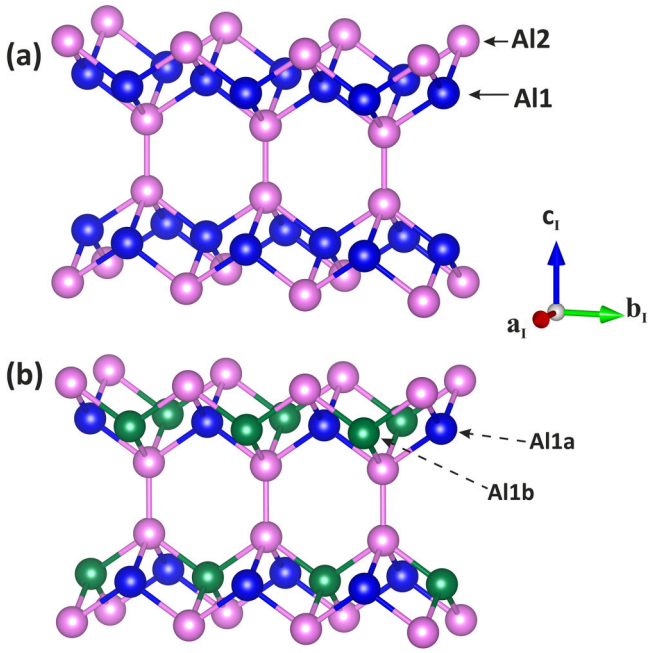

FIG. 5. Perspective view of layers of aluminum atoms in $EuAl_4$. (a) Layer of Al atoms in the periodic phase, where the shortest distances are within the Al2-Al2 dumbbells with d[Al2–Al2] = 2.562(3) Å at 160 K. Next shortest distances are d[Al2–Al1] = 2.666(2) Å and d[Al1–Al1] = 3.1058(1) Å. (b) The CDW phase featuring Al1a and Al1b independent atoms in the basic structure of symmetry $F222$. Basic-structure distances in the modulated CDW phase at 30 K are d[Al2–Al2] = 2.566(2) Å, d[Al2–Al1a] = d[Al2–Al1b] = 2.662(1) Å, and d[Al1a–Al1b] = 3.1027 Å. The modulation of these distances is given as t-plots in Fig. 7.

coordinate axes of $I4/mmm$, and the F-centered orthorhombic groups preserve the diagonal twofold axes of $I4/mmm$. We believe that the distinction could be made between all six possible superspace groups in Table II, because the present SXRD-30 diffraction data is an extensive data set containing second-order satellite reflections. Although observed, previous structural analysis was based on SXRD data containing only first-order satellite reflections [21,22]. The finding of acentric symmetry is in agreement with the isostructural, nonmagnetic compound $SrAl_4$, which features a stronger CDW with stronger second-order satellites, that are also described by the acentric superspace group $F222(0\,0\,\sigma)00s$ [28]. The absence of inversion symmetry immediately implies that the previously reported skyrmion lattices could be stabilized by the DM interaction and do not need more exotic mechanisms [17,18,27,29].

Whereas the choice of $F222(0\,0\,\sigma)00s$ is principally based on the quality of the fit to the SXRD data of the CDW phase, the structure refinement also leads to a structure model for the CDW phase of $EuAl_4$. First, it is to be noted that the basic structure remains $I4/mmm$ (Table S6 in [38]). Only ADP parameters could deviate from this symmetry, but they were fixed to the tetragonal symmetry, because a lower symmetry of the ADP parameters is unlikely for a crystal structure that lacks distortions. The lower symmetry, including the loss of inversion symmetry, thus is entirely due to the symmetry of the CDW modulation. Such a phenomenon has been observed before, for example for Mo_2S_3 [44], $Sm_2Ru_3Ge_5$ [45], and $Gd_2Os_3Si_5$ [46]. Presently, the CDW modulation represents a transverse wave (Table S7 in [38]), in agreement with [25].

A second point to notice is that the two centrosymmetric orthorhombic superspace groups as well as the acentric tetragonal superspace groups are not subgroups of any superspace group based on $I4/mmm$. On the other hand, $F222(0\,0\,\sigma)00s$ is a subgroup of both $F422(0\,0\,\sigma)q00$ and, previously proposed, $Fmmm(0\,0\,\sigma)s00$ (Fig. 4). Indeed, the present acentric structure model can be considered as a distortion of the $Fmmm(0\,0\,\sigma)s00$ model (compare the discussion in Sec. S6 in the Supplemental Material [38]). Initially, it appears that all atoms exhibit similar displacements along $\mathbf{a}_F$ [Figs. 5 and 6(a), and Table S7 and Figs. S1–S3 in [38]]. However, major effect is the unequal displacement modulations of the Al1a and Al1b atoms into the direction of $\mathbf{b}_F$ [Figs. 5 and 6(b), and Table S7 and Figs. S1–S3 in [38]]. t-Plots reveal that the major modulation of interatomic distances is between Al1 atoms and of secondary importance between Al2 and Al1 atoms (Fig. 7). This finding is in agreement with the $Fmmm(0\,0\,\sigma)s00$ model [21], and it confirms that the CDW resides on the aluminum layers [47,48]. The acentric distortion of the CDW according to $F222(0\,0\,\sigma)00s$ appears to be in agreement with the structure proposed by Ni *et al.* [27] on the basis of 4D-STEM data, although in the latter report no symmetry group was given (see the discussion in Sec. S7 of the Supplemental Material [38]).

Korshunov *et al.* [22] have proposed for the CDW phase of $EuAl_4$ the centrosymmetric superspace group $Immm(0\,0\,\sigma)s00$. We have recently found this symmetry for the CDW phase of $EuAl_2Ga_2$ [24]. In view of the present results for $EuAl_4$, it is likely that the true symmetry of $EuAl_2Ga_2$ could be $I222(0\,0\,\sigma)00s$, since the analyses in [22] and [24] were based on SXRD data without second-order satellite reflections, for which it is difficult to distinguish acentric from centrosymmetric symmetries. Also, consideration of the four orthorhombic symmetries listed in Fig. 4 and Table II shows that they share the tetragonal basic structure as well as a modulation that is strongest on the layers of Al1 atoms (compare to Sec. S5 in [38]) [21,28]. Therefore, it is conceivable that the CDWs can be stabilized by modulations according to either of these symmetries. It is then possible that $F222(0\,0\,\sigma)00s$ is most stable for $EuAl_4$, while $I222(0\,0\,\sigma)00s$ is most stable for $EuAl_2Ga_2$. It might even be the case that a different symmetry is achieved for the CDW state of a single compound, depending on its chemical purity and the concentration of lattice defects.

A modulation of the ADPs was required, in order to resolve the ΔF problem of the second-order satellite reflections. Structure refinements have shown that first-order harmonic modulation parameters were without effect and refined to value zero, while the second-order harmonic modulation parameters lead to the good fit to the SXRD-30 data. Pérez-Mato *et al.* [26] have shown that second-order harmonic modulation of ADPs reflects the presence of phasons in the incommensurate modulation wave. Therefore, we propose that the CDW

TABLE III. Structure refinements against the SXRD-70 data of $EuAl_4$ in its incommensurate CDW phase at $T = 70$ K. Data from [21]. The same types of structure model and the same symmetries are considered as in Table II. The SXRD-70 data have been processed according to the centrosymmetric point group $2/m$ (**c** unique; Table S1 in [38]). Criterion of observability is $I > 3\sigma(I)$. n_{par} is the number of refined parameters. A ΔF-problem does not exist, because second-order satellites are not part of the SXRD-70 data.

SSG	Averaging	n_{par}	R_F^{obs} (Overall) (%)	R_F^{obs} ($m = 0$) (%)	R_F^{obs} ($m = 1$) (%)	R_F^{all} (all) (%)
			Basic structure			
$I422(0\,0\,\sigma)q00$	$2/m$	9	2.05	2.05		2.05
$I4(0\,0\,\sigma)q00$	$2/m$	11	2.03	2.03		2.03
$Immm(0\,0\,\sigma)s00$	$2/m$	9	2.05	2.05		2.05
$I222(0\,0\,\sigma)00s$	$2/m$	9	2.05	2.05		2.05
$Fmmm(0\,0\,\sigma)s00$	$2/m$	9	2.05	2.05		2.05
$F222(0\,0\,\sigma)00s$	$2/m$	9	2.05	2.05		2.05
			Displacement modulation			
$I422(0\,0\,\sigma)q00$	$2/m$	14	3.21	2.06	6.22	3.38
$I4(0\,0\,\sigma)q00$	$2/m$	21	3.19	2.04	6.17	3.38
$Immm(0\,0\,\sigma)s00$	$2/m$	16	3.2	2.13	5.99	3.36
$I222(0\,0\,\sigma)00s$	$2/m$	21	3.15	2.09	5.92	3.33
$Fmmm(0\,0\,\sigma)s00$	$2/m$	15	3.14	2.16	5.7	3.28
$F222(0\,0\,\sigma)00s$	$2/m$	19	3.2	2.06	6.18	3.37
			Displacement + ADP modulation			
$I422(0\,0\,\sigma)q00$	$2/m$	24	3.01	2.07	5.45	3.22
$I4(0\,0\,\sigma)q00$	$2/m$	41	2.79	1.85	5.22	2.98
$Immm(0\,0\,\sigma)s00$	$2/m$	31	2.74	1.97	4.73	3.07
$I222(0\,0\,\sigma)00s$	$2/m$	41	2.46	1.65	4.56	2.64
$Fmmm(0\,0\,\sigma)s00$	$2/m$	28	2.76	2.02	4.7	2.96
$F222(0\,0\,\sigma)00s$	$2/m$	40	2.41	1.67	4.34	2.59

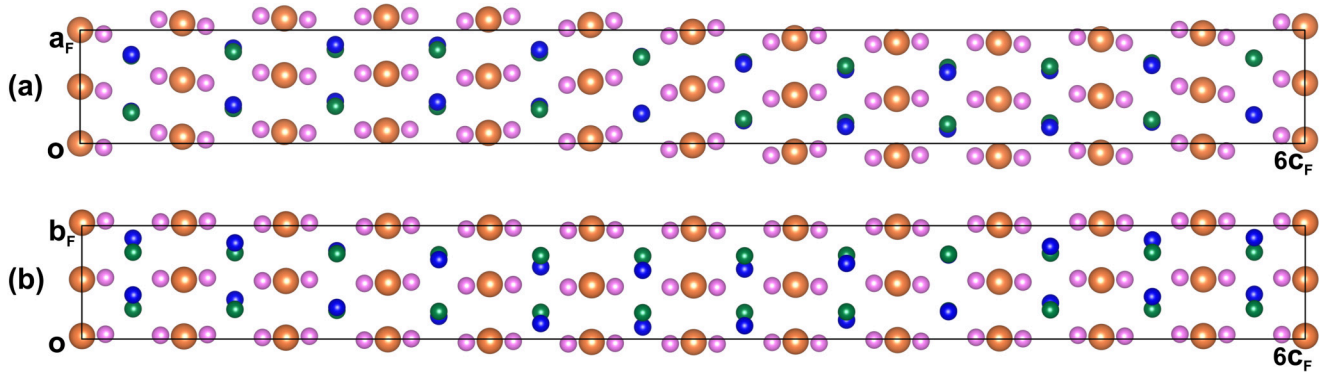

FIG. 6. Incommensurately modulated crystal structure of $EuAl_4$ for symmetry $F222(0\,0\,\sigma)00s$ (Table I). Black lines represent the boundary of $1 \times 1 \times 6$ unit cells of the basic structure. All atoms are at their modulated (displaced) positions. Eu in orange, Al1a in blue, Al1b in green, and Al2 in pink. (a) Projection along $\mathbf{b}_F$, showing displacements along $\mathbf{a}_F$. (b) Projection along $\mathbf{a}_F$, showing displacements along $\mathbf{b}_F$. Atomic displacements have been magnified by a factor of five. Displacements are zero along $\mathbf{c}_F$.

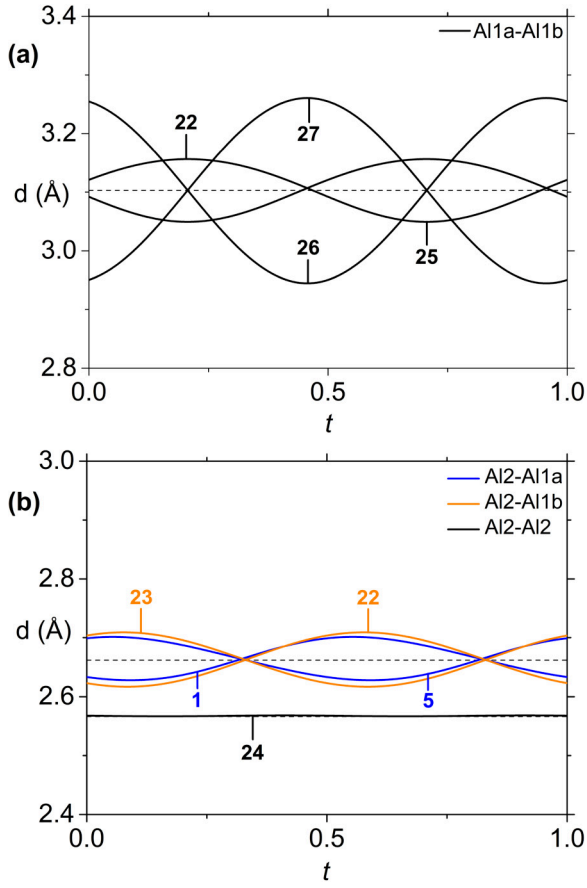

FIG. 7. t-Plots of interatomic distances (Å) in the CDW phase of $EuAl_4$ at 30 K. (a) d[Al1a–Al1b] with Al1a as central atom, and (b) d[Al2–Al1a], d[Al2–Al1b], and d[Al2–Al2] with Al2 as central atom. Basic structure distances are indicated by the dashed horizontal lines. t-Plots display variation in atomic parameters such as distance and position as a function of the phase t of the modulation wave [42]. Here, each value of t gives the distances from a central atom toward its neighboring atoms. The number on each curve is the number of the symmetry operator that is applied to the second atom of the bond pair. Symmetry operators are listed in Table S9 in the Supplemental Material [38].

modulation in $EuAl_4$ and related compounds includes phason disorder.

V. CONCLUSIONS

Broken inversion symmetry of the CDW phase is established for $EuAl_4$. Essential experimental information was the presence of second-order satellites in the SXRD data set. The CDW modulation is transverse, like it was found for isostructural $SrAl_4$ [28], and it is best described by the acentric orthorhombic superspace group $F222(0\,0\,\sigma)00s$. Despite conflicting conclusions, $F222(0\,0\,\sigma)00s$ appears to be in agreement with all experimental results on $EuAl_4$ [21–23,25,27].

The CDW is found to reside on the Al–Al network, in agreement with previous models. The acentric nature of the CDW modulation is most clearly established by the unequal modulations of the Al1a and Al1b atoms. It should be considered, when considering models for the stabilization of the skyrmion states of $EuAl_4$.

ACKNOWLEDGMENTS

Single crystals of $EuAl_4$ were grown by Kerstin Küspert at the Laboratory of Crystallography in Bayreuth. We thank Kerstin Küspert and Carsten Paulmann for their assistance in data collection at beamline P24. We acknowledge DESY (Hamburg, Germany), a member of the Helmholtz Association HGF, for the provision of experimental facilities. Beamtime was allocated for Proposal No. I-20231047. S.R. thanks the Agence Nationale de la Recherche for support within the project SUPERNICKEL (Grant No. ANR-21-CE30-0041). This research has been funded by the Deutsche Forschungsgemeinschaft (DFG, German Research Foundation)–406658237.

DATA AVAILABILITY

The data that support the findings of this article are not publicly available. The data are available from the authors upon reasonable request.

[1] G. Grüner, *Charge Density Waves in Solids* (Addison-Wesley, Reading, Massachusetts, 1994).

[2] P. Monceau, Electronic crystals: an experimental overview, Adv. Phys. **61**, 325 (2012).

[3] J.-P. Pouget and E. Canadell, Structural approach to charge density waves in low-dimensional systems: electronic instability and chemical bonding, Rep. Prog. Phys. **87**, 026501 (2024).

[4] D. I. Khomskii and S. V. Streltsov, Orbital effects in solids: Basics, recent progress, and opportunities, Chem. Rev. **121**, 2992 (2021).

[5] H. D. Yang, P. Klavins, and R. N. Shelton, Competition between superconductivity and charge-density-waves in the pseudoternary system $(Lu_{1-x}Sc_x)_5Ir_4Si_{10}$, Phys. Rev. B **43**, 7681 (1991).

[6] S. Ramakrishnan and S. van Smaalen, Unusual ground states in $R_5T_4X_{10}$ (R = rare earth; T = Rh, Ir; and X = Si, Ge, Sn): a review, Rep. Prog. Phys. **80**, 116501 (2017).

[7] Q. Wang, P. Kong, W. Shi, C. Pei, C. Wen, L. Gao, Y. Zhao, Q. Yin, Y. Wu, G. Li, H. Lei, J. Li, Y. Chen, S. Yan, and Y. Qi, Charge density wave orders and enhanced superconductivity under pressure in the kagome metal CsV_3Sb_5, Adv. Mater. **33**, 2102813 (2021).

[8] Y. Xie, Y. Li, P. Bourges, A. Ivanov, Z. Ye, J.-X. Yin, M. Z. Hasan, A. Luo, Y. Yao, Z. Wang, G. Xu, and P. Dai, Electron-phonon coupling in the charge density wave state of CsV_3Sb_5, Phys. Rev. B **105**, L140501 (2022).

[9] K. K. Kolincio, M. Roman, M. J. Winiarski, J. Strychalska-Nowak, and T. Klimczuk, Magnetism and charge density waves in $RNiC_2$ (R = Ce, Pr, Nd), Phys. Rev. B **95**, 235156 (2017).

[10] M. Roman, M. Fritthum, B. Stöger, D. T. Adroja, and H. Michor, Charge density wave and crystalline electric field effects in $TmNiC_2$, Phys. Rev. B **107**, 125137 (2023).

[11] S. Shimomura, C. Hayashi, G. Asaka, N. Wakabayashi, M. Mizumaki, and H. Onodera, Charge-density-wave destruction

and ferromagnetic order in $SmNiC_2$, Phys. Rev. Lett. **102**, 076404 (2009).

[12] A. Wölfel, L. Li, S. Shimomura, H. Onodera, and S. van Smaalen, Commensurate charge-density wave with frustrated interchain coupling in $SmNiC_2$, Phys. Rev. B **82**, 054120 (2010).

[13] S. Ramakrishnan, A. Schönleber, T. Rekis, N. van Well, L. Noohinejad, S. van Smaalen, M. Tolkiehn, C. Paulmann, B. Bag, A. Thamizhavel, D. Pal, and S. Ramakrishnan, Unusual charge density wave transition and absence of magnetic ordering in $Er_2Ir_3Si_5$, Phys. Rev. B **101**, 060101(R) (2020).

[14] Y. Singh, D. Pal, and S. Ramakrishnan, Low-temperature studies of the magnetic and superconducting properties of the $R_2Ir_3Si_5$ (R = Y, La, Ce–Nd, Gd–Tm) system, Phys. Rev. B **70**, 064403 (2004).

[15] J. M. Moya, S. Lei, E. M. Clements, C. S. Kengle, S. Sun, K. Allen, Q. Li, Y. Y. Peng, A. A. Husain, M. Mitrano, M. J. Krogstad, R. Osborn, A. B. Puthirath, S. Chi, L. Debeer-Schmitt, J. Gaudet, P. Abbamonte, J. W. Lynn, and E. Morosan, Incommensurate magnetic orders and topological Hall effect in the square-net centrosymmetric $EuGa_2Al_2$ system, Phys. Rev. Mater. **6**, 074201 (2022).

[16] A. M. Vibhakar, D. D. Khalyavin, J. M. Moya, P. Manuel, F. Orlandi, S. Lei, E. Morosan, and A. Bombardi, Competing charge and magnetic order in the candidate centrosymmetric skyrmion host $EuGa_2Al_2$, Phys. Rev. B **108**, L100404 (2023).

[17] R. Takagi, N. Matsuyama, V. Ukleev, L. Yu, J. S. White, S. Francoual, J. R. L. Mardegan, S. Hayami, H. Saito, K. Kaneko, K. Ohishi, Y. Ōnuki, T.-h. Arima, Y. Tokura, T. Nakajima, and S. Seki, Square and rhombic lattices of magnetic skyrmions in a centrosymmetric binary compound, Nat. Commun. **13**, 1472 (2022).

[18] M. Gen, R. Takagi, Y. Watanabe, S. Kitou, H. Sagayama, N. Matsuyama, Y. Kohama, A. Ikeda, Y. Onuki, T. Kurumaji, T.-h. Arima, and S. Seki, Rhombic skyrmion lattice coupled with orthorhombic structural distortion in $EuAl_4$, Phys. Rev. B **107**, L020410 (2023).

[19] R. Yang, C. C. Le, P. Zhu, Z. W. Wang, T. Shang, Y. M. Dai, J. P. Hu, and M. Dressel, Charge density wave transition in the magnetic topological semimetal $EuAl_4$, Phys. Rev. B **109**, L041113 (2024).

[20] S. Shimomura, H. Murao, S. Tsutsui, H. Nakao, A. Nakamura, M. Hedo, T. Nakama, and Y. Ōnuki, Lattice modulation and structural phase transition in the antiferromagnet $EuAl_4$, J. Phys. Soc. Jpn. **88**, 014602 (2019).

[21] S. Ramakrishnan, S. R. Kotla, T. Rekis, J.-K. Bao, C. Eisele, L. Noohinejad, M. Tolkiehn, C. Paulmann, B. Singh, R. Verma, B. Bag, R. Kulkarni, A. Thamizhavel, B. Singh, S. Ramakrishnan, and S. van Smaalen, Orthorhombic charge density wave on the tetragonal lattice of $EuAl_4$, IUCrJ **9**, 378 (2022).

[22] A. N. Korshunov, A. S. Sukhanov, S. Gebel, M. S. Pavlovskii, N. D. Andriushin, Y. Gao, J. M. Moya, E. Morosan, and M. C. Rahn, Phonon softening and atomic modulations in $EuAl_4$, Phys. Rev. B **110**, 045102 (2024).

[23] A. S. Sukhanov, S. Gebel, A. N. Korshunov, N. D. Andriushin, M. S. Pavlovskii, Y. Gao, J. M. Moya, K. Allen, E. Morosan, and M. C. Rahn, Electron-phonon coupling in $EuAl_4$ under hydrostatic pressure, Phys. Rev. B **111**, 195150 (2025).

[24] H. Agarwal, S. R. Kotla, L. Noohinejad, B. Bag, C. Eisele, S. Ramakrishnan, M. Tolkiehn, C. Paulmann, A. Thamizhavel, S. Ramakrishnan, and S. van Smaalen, *I*-centered versus *F*-centered orthorhombic symmetry and negative thermal expansion of the charge density wave of $EuAl_2Ga_2$, Phys. Rev. B **111**, 155144 (2025).

[25] F. Z. Yang, K. F. Luo, W. Zhang, X. Guo, W. R. Meier, H. Ni, H. X. Li, P. M. Lozano, G. Fabbris, A. H. Said, C. Nelson, T. T. Zhang, A. F. May, M. A. McGuire, R. Juneja, L. Lindsay, H. N. Lee, J. M. Zuo, M. F. Chi, X. Dai *et al.*, Incommensurate transverse Peierls transition, arXiv:2410.10539.

[26] J. Pérez-Mato, G. Madariaga, and L. Elcoro, Influence of phason dynamics on atomic Debye-Waller factors of incommensurate modulated structures and quasicrystals, Solid State Commun. **78**, 33 (1991).

[27] H. Ni, W. R. Meier, H. Miao, A. F. May, B. C. Sales, J.-M. Zuo, and M. Chi, Real-space visualization of atomic displacements in a long-wavelength charge density wave using cryogenic 4D-STEM, Phys. Rev. Mater. **8**, 104414 (2024).

[28] S. Ramakrishnan, S. R. Kotla, H. Pi, B. B. Maity, J. Chen, J.-K. Bao, Z. Guo, M. Kado, H. Agarwal, C. Eisele, M. Nohara, L. Noohinejad, H. Weng, S. Ramakrishnan, A. Thamizhavel, and S. van Smaalen, Noncentrosymmetric, transverse structural modulation in $SrAl_4$, and elucidation of its origin in the $BaAl_4$ family of compounds, Phys. Rev. Res. **6**, 023277 (2024).

[29] S. Mühlbauer, B. Binz, F. Jonietz, C. Pfleiderer, A. Rosch, A. Neubauer, R. Georgii, and P. Boni, Skyrmion lattice in a chiral magnet, Science **323**, 915 (2009).

[30] N. Nagaosa and Y. Tokura, Topological properties and dynamics of magnetic skyrmions, Nat. Nanotechnol. **8**, 899 (2013).

[31] Y. Tokura and N. Kanazawa, Magnetic skyrmion materials, Chem. Rev. **121**, 2857 (2021).

[32] A. M. Vibhakar, D. D. Khalyavin, F. Orlandi, J. M. Moya, S. Lei, E. Morosan, and A. Bombardi, Spontaneous reversal of spin chirality and competing phases in the topological magnet $EuAl_4$, Commun. Phys. **7**, 313 (2024).

[33] A. Nakamura, T. Uejo, F. Honda, T. Takeuchi, H. Harima, E. Yamamoto, Y. Haga, K. Matsubayashi, Y. Uwatoko, M. Hedo, T. Nakama, and Y. Ōnuki, Transport and magnetic properties of $EuAl_4$ and $EuGa_4$, J. Phys. Soc. Jpn. **84**, 124711 (2015).

[34] D. Pennicard, S. Lange, S. Smoljanin, H. Hirsemann, and H. Graafsma, LAMBDA–large area Medipix3-based detector array, J. Instrum. **7**, C11009 (2012).

[35] Rigaku, CrysAlis^{Pro} version 171.40.53, Rigaku Oxford diffraction (2019), https://rigaku.com/products/crystallography/x-ray-diffraction/crysalispro.

[36] A. M. M. Schreurs, X. Xian, and L. M. J. Kroon-Batenburg, *EVAL15*: a diffraction data integration method based on *ab initio* predicted profiles, J. Appl. Crystallogr. **43**, 70 (2010).

[37] G. M. Sheldrick, *SADABS, Version 2008/1* (Germany Bruker AXS Inc., Karlsruhe, 2008).

[38] See Supplemental Material at http://link.aps.org/supplemental/10.1103/kl2z-brms for details on the diffraction experiments and values of the structural parameters.

[39] V. Petříček, L. Palatinus, J. Plasil, and M. Dusek, JANA2020–a new version of the crystallographic computing system JANA, Z. Kristallogr. Cryst. Mater. **238**, 271 (2023).

[40] H. T. Stokes, B. J. Campbell, and S. van Smaalen, Generation of $(3+d)$-dimensional superspace groups for describing the symmetry of modulated crystalline structures, Acta Crystallogr. A **67**, 45 (2011).

[41] T. Shang, Y. Xu, S. Gao, R. Yang, T. Shiroka, and M. Shi, Experimental progress in $Eu(Al,Ga)_4$ topological antiferromagnets, J. Phys.: Condens. Matter **37**, 013002 (2025).

[42] S. van Smaalen, *Incommensurate Crystallography* (Oxford University Press, Oxford, 2012).

[43] T. Janssen, G. Chapuis, and M. de Boissieu, *Aperiodic Crystals: From Modulated Phases to Quasicrystals*, 2nd ed. (Oxford University Press, Oxford, 2018).

[44] W. J. Schutte, F. Disselborg, and J. L. de Boer, Determination of the two-dimensional incommensurately modulated structure of Mo_2S_3, Acta Crystallogr. B **49**, 787 (1993).

[45] D. E. Bugaris, C. D. Malliakas, F. Han, N. P. Calta, M. Sturza, M. J. Krogstad, R. Osborn, S. Rosenkranz, J. P. C. Ruff, G. Trimarchi, S. L. Bud'ko, M. Balasubramanian, D. Y. Chung, and M. G. Kanatzidis, Charge density wave in the new polymorphs of $RE_2Ru_3Ge_5$ (RE = Pr, Sm, Dy), J. Am. Chem. Soc. **139**, 4130 (2017).

[46] V. Sharma, S. Ramakrishnan, J. SS, S. R. Kotla, B. Maiti, C. Eisele, H. Agarwal, L. Noohinejad, M. Tolkiehn, D. Bansal, S. van Smaalen, and T. Arumugam, Room temperature charge density wave in a tetragonal polymorph of $Gd_2Os_3Si_5$ and study of its origin in the $RE_2T_3X_5$ (RE = rare earth, T = transition metal, X = Si, Ge) series, Chem. Mater. **36**, 6888 (2024).

[47] M. Kobata, S.-i. Fujimor, Y. Takeda, T. Okane, Y. Saitoh, K. Kobayashi, H. Yamagami, A. Nakamura, M. Hedo, T. Nakama, and Y. Onuki, Electronic structure of $EuAl_4$ studied by photoelectron spectroscopy, J. Phys. Soc. Jpn. **85**, 094703 (2016).

[48] K. Kaneko, T. Kawasaki, A. Nakamura, K. Munakata, A. Nakao, T. Hanashima, R. Kiyanagi, T. Ohhara, M. Hedo, T. Nakama, and Y. Ōnuki, Charge-density-wave order and multiple magnetic transitions in divalent europium compound $EuAl_4$, J. Phys. Soc. Jpn. **90**, 064704 (2021).